Intermittency assessed through a model of kurtosis-skewness relation in MHD in fast dynamo regimes

Yannick Ponty, Hélène Politano, Annick Pouquet

Intermittency assessed through a model of kurtosis-skewness relation in MHD in fast dynamo regimes

Yannick Ponty[1]†, Hélène Politano[2] and Annick Pouquet[3]

[1]Université Côte d'Azur, CNRS, Observatoire de la Côte d'Azur, Laboratoire Lagrange, France
[2]Université Côte d'Azur, CNRS, Laboratoire J. A. Dieudonné, France
[3]National Center for Atmospheric Research, P.O. Box 3000, Boulder, CO 80307, USA

(Received xx; revised xx; accepted xx)

Intermittency as it occurs in fast dynamos in the MHD framework is evaluated through the examination of relations between normalized moments at third order (skewness S) and fourth order (kurtosis K) for both the velocity and magnetic field, and for their local dissipations. As investigated by several authors in various physical contexts such as fusion plasmas (Krommes (2008)), climate evolution (Sura & Sardeshmukh (2008)), fluid turbulence or rotating stratified flows (Pouquet *et al.* (2023)), approximate parabolic $K(S) \sim S^\alpha$ laws emerge whose origin may be related to the applicability of intermittency models to their dynamics. The results analyzed herein are obtained through direct numerical simulations of MHD flows for both Taylor-Green and Beltrami ABC forcing at moderate Reynolds numbers, and for up to 3.14×10^5 turn-over times. We observe for the dissipation $0.2 \lesssim \alpha \lesssim 3.0$, an evaluation that varies with the field, the forcing, and when filtering for high-skewness intermittent structures. When using the She & Lévêque (1994) intermittency model, one can compute α analytically; we then find $\alpha \approx 2.5$, clearly differing from a (strict) parabolic scaling, a result consistent with the numerical data.

Key words: MHD; Fast dynamo; Intermittency; Kurtosis; Dissipation; Turbulence

1. Introduction

One striking property of turbulent flows is their lack of predictability, as well as their intermittency, associated with the presence of intense and isolated patterns at small scales, such as vortex filaments and current sheets, or coherent structures at large scale. Such extreme events can be assessed through their probability distribution functions (PDFs), and thus through their normalized moments such as the skewness and kurtosis (definitions are given in §3). These intense structures have been identified in many experiments, observations and direct numerical simulations (see for recent reviews *e.g.* Matthaeus *et al.* (2015); Yeung *et al.* (2015); Chen (2016); Camporeale *et al.* (2018); Ergun *et al.* (2020); Schekochihin (2022)). The ensuing dissipation is found in a reduced volume of the system, in both neutral fluids (Bradshaw *et al.* (2019); Rafner *et al.* (2021); Buaria *et al.* (2022)) and MHD (see *e.g.* Politano *et al.* (1995); Meneguzzi *et al.* (1996); Mallet *et al.* (2017); Zhdankin *et al.* (2017); Adhikari *et al.* (2020)). This physical intermittency volume can be in fact smaller than for fully developed turbulence (FDT) in the presence of gravity waves (Marino *et al.* (2022)), as also found in clear air turbulence, and similar observations are documented for plasma disruptions.

† Email address for correspondence: yannick.ponty@oca.eu

Intermittency can be characterized in many ways, such as when evaluating anomalous exponents of structure functions. Perhaps more directly, one can assess when and where normalized third and fourth-order moments, skewness S and kurtosis K, differ from their Gaussian value. There is a long history of such measurements; for example, both skewness and kurtosis, have been used to map a flow, such as in meandering jets in the ocean (Hughes *et al.* (2010)), or in climate data reanalysis (Petoukhov *et al.* (2008)).

One way to condense the data further is to look for $K(S)$ relations, often found to be close to parabolic in a variety of contexts (see Pouquet *et al.* (2023) and references therein for a recent review), for the Navier-Stokes (NS) equations, in presence or not of stratification and/or rotation, as relevant to the atmosphere, the ocean and climate (Lenschow *et al.* (1994); Sura & Sardeshmukh (2008)). Such quasi-parabolic laws were also found in laboratory and astrophysical plasmas (see *e.g.* Labit *et al.* (2007); Krommes (2008); Sattin *et al.* (2009); Garcia (2012); Guszejnov *et al.* (2013); Mezaoui *et al.* (2014); Furno *et al.* (2015); Miranda *et al.* (2018)). More recently, Sladkomedova *et al.* (2023) analysed the intermittency of the density in MAST (Mega Ampere Spherical Tokamak) plasmas, and found that the data agrees with the $K(S)$ model given by Garcia (2012) (see also Guszejnov *et al.* (2013); Losada *et al.* (2023)). †

Detailed knowledge of intermittency in plasmas and turbulent systems in general may lead to a better understanding of their PDFs and of the dissipation mechanisms at play. It is in this context that we want to examine in this paper the intermittent properties of MHD through the possible relationship between excess kurtosis and skewness for the velocity and magnetic field, as well as for their local dissipation. MHD has, of course, many different regimes, and we concentrate here on one subset, namely that of the fast dynamo in its nonlinear phase and at moderate Reynolds number for which long runs are available, up to in excess of $10^5\tau_{nl}$, where $\tau_{nl} = L_{int}/V_{rms}$ is the turn-over time of the turbulence based on the large-scale velocity V_{rms} and on the integral length scale L_{int}. In the next section, we summarize the framework utilizing Langevin equations to yield such intermittency, and in §3 are written the equations and definitions needed for our analysis of MHD numerical data for a fast dynamo regime, as well as information on the direct numerical simulations (DNSs) employed herein. In Section §4, we analyze the results and give an interpretation within a specific model of intermittency, and the last section presents a discussion and our conclusions.

2. A Langevin framework for a $K(S)$ parabolic behavior

2.1. *The linear case*

A $K(S)$ parabolic law has been derived explicitly in Sura & Sardeshmukh (2008) for a model of oceanic sea-surface temperature anomalies (SST), based on the dynamics of a specific linear Langevin model with both additive and multiplicative noises. Analyzing the corresponding Fokker-Planck equation for the stationary PDF, these authors can show analytically that in the limit of weak multiplicative noise, $K(S) \sim 3S^2/2$. Multiple other studies show the plausibility of a Langevin model for parabolic $K(S)$ behaviors in different contexts as exemplified in Hasselmann (1962); Sattin *et al.* (2009) (see also Farago (2002); Farrell & Ioannou (2009)), with a fast and weak multiplicative noise due to the emergence of rapid small-scale and thus (on average) low-amplitude eddies. The kinematic dynamo equations, with a given fixed possibly stochastic and delta-correlated

† The model is based on moments up to fourth order as well as on an estimate of the number of the intermittent events that are observed simultaneously.

in time velocity field, lend themselves naturally to the Langevin framework (see *e.g.* Watkins *et al.* (2016) for a link with self-organized criticality).

Models in the case of fusion plasmas have also been written, for example in the context of magnetically-confined experiments. In Garcia (2012), the dynamics, as for dissipation events, is viewed as a random sequence of bursts as opposed to a quasi-continuum. These bursts are occurring independently and following a Poisson process. When taking for the shape of these bursts a sharp rise and a slow exponential decay, one can compute $K(S)$ relations which, for an exponential distribution of burst amplitudes, becomes $K(S) = 3S^2/2$ where the $3/2$ coefficient can be modified by the presence of added noise (see also Theodorsen *et al.* (2017)).

2.2. *The nonlinear regime of the dynamo*

In the saturation phase of the dynamo, the equations are now nonlinear. Nonlinear Langevin equations are already studied in Zwanzig (1973). Several Langevin approaches in MHD have been derived as well in the nonlinear case. For example, a sub-diffusive behavior was unraveled in Balescu *et al.* (1994), from first principles, in the context of a stochastic magnetic field. One can also choose to add a cubic term in the induction equation (cubic so that the symmetry of the axial magnetic field be preserved), in order to mimic the effect the Lorentz force has on the velocity (see *e.g.* Boldyrev (2001); Leprovost & Dubrulle (2005)), in particular for large magnetic Prandtl numbers. On the other hand, it was shown in Nazarenko *et al.* (2000) that in the case of the fast dynamo, the feed back of the growing induction is through the creation of counter-rotating vortices, a point not included in a saturation involving only the magnetic field equation.

One can also consider the role of Alfvén waves in the nonlinear regime by introducing in a linear Langevin equation an oscillatory term (Bandyopadhyay *et al.* (2018)). Certainly, one of the main effect of a magnetic field, in both the linear and nonlinear regimes, is that its large-scale component is responsible for bringing into equipartition large-scale and small-scale velocity and induction, as shown already using a non-helical version of a two-point closure in MHD (Kraichnan & Nagarajan (1967)). However, in the present paper examining a chaotic small-scale dynamo regime, the large-scale magnetic field is not expected to be strong in the absence of overall helicity, and of scale separation, and thus the Alfvén waves it would produce are not likely going to be substantially faster than the eddy turn-over time τ_{nl} or, said differently, we are not in a regime of weak MHD turbulence so that the waves will likely not modify or impede significantly the turbulence regime and the ensuing intermittency. In a Langevin equation, in a sense, one is getting rid of the closure problem for turbulent motions since it is linear, with the complex nonlinear small-scale dynamics bundled up in a rapid stochastic forcing with an assumption of (mostly) local interactions among these fast motions.

Another question is whether the intermittency of the early dissipation range dominates the statistics, at least at moderate Reynolds numbers. Indeed, one could argue that the intermittency of the dissipation is mostly located in the beginning of the range, due to the ensuing fast decay. In Wu *et al.* (2023), a near-dissipation range intermittency is examined using Solar Wind data obtained with the Parker Solar Probe. The authors conclude that they find evidence for log-Poisson scaling as modeled for MHD in Grauer *et al.* (1994); Politano & Pouquet (1995), and that such structures are also almost entirely responsible for the intermittency anisotropy (see also Bian & Li (2024)). This may be consistent with stating, as developed already in Kraichnan (1967), that most of the intermittency is in fact at the beginning of the dissipative range.

3. Equations and numerical set-up

3.1. *Equations and definitions*

The equations for MHD in the incompressible case are written as usual as:

$$[\partial_t + \mathbf{u}\cdot\nabla]\mathbf{u} \equiv D_t\mathbf{u} = -\nabla P^\star + \mathbf{b}\cdot\nabla\mathbf{b} + \nu\Delta\mathbf{u} + \mathbf{F}_V, \tag{3.1}$$

$$[\partial_t + \mathbf{u}\cdot\nabla]\mathbf{b} \equiv D_t\mathbf{b} = \mathbf{b}\cdot\nabla\mathbf{u} + \eta\Delta\mathbf{b}, \tag{3.2}$$

together with $\nabla\cdot\mathbf{u} = 0, \nabla\cdot\mathbf{b} = 0$; $\mathbf{u}, \mathbf{b}$ are the velocity and magnetic field (in Alfvén velocity units), $P^\star$ is the total pressure, ν, η are the viscosity and magnetic diffusivity, and $\mathbf{F}_V$ is a forcing term. We will use in this paper two types of forcing. The first one is the ABC (Arnold-Beltrami-Childress) forcing, which is a superposition of Beltrami vortices and thus fully helical; it is defined as:

$$\mathbf{f}_{\rm ABC} = [\cos(y) + \sin(z)]\,\hat{x} + [\sin(x) + \cos(z)]\,\hat{y} + [\cos(x) + \sin(y)]\,\hat{z}. \tag{3.3}$$

The ABC flow is an eigenfunction of the curl, and it is an exact solution of the Euler equations; thus, for large enough viscosity, it is stable but turbulence develops as the Reynolds number R_V increases. We also take the Taylor-Green (TG) forcing written as:

$$\mathbf{f}_{\rm TG} = f_0^{tg}\left\{[\sin x\ \cos y\ \cos z]\,\hat{x} - [\cos x\ \sin y\ \cos z]\,\hat{y} + 0\hat{z}\right\}\ , \tag{3.4}$$

with $f_0^{tg} = 3$. This forcing is globally nonhelical, but it can be viewed in fact as an assembly of helical patches of both signs and varied intensities.

We solved numerically our MHD system in a fully periodic box using a classic pseudo-spectral solver, involving a 2/3 dealiasing technique with a parallel CPU-MPI code (CUBBY; Ponty *et al.* (2005)). With these two forcings, we compute four simulations altogether, for up to hundreds of thousands of eddy turn over times, and we record the same amount of snapshots for the six three-dimensional field components. Some of the data and a few of the statistical properties of these runs are given in Table.3.1.

3.2. *Rapid description of the runs*

The dynamo problem, concerning the generation of magnetic fields at both large and small scales, is a long-standing topic (see Brandenburg & Subramanian (2005); Rincon (2019) for thorough recent reviews). In the context of this paper, we analyze four simulation runs, focusing on the turbulent dynamo regime. In these simulations, the (fast) dynamo is triggered when the magnetic Reynolds number R_M exceeds a threshold that depends on the magnetic Prandtl number $P_m = \nu/\eta$ (Ponty *et al.* (2005)), as seen in run TG3. Sub-critical dynamos can also be observed, where magnetically-induced changes to the velocity field play a role, such as in run TG1 which is close to the onset of dynamo action, and living on the sub-critical branch (Ponty *et al.* (2007)). It is also worth noting that the Lorenz force's feedback on the velocity field can influence the so-called "on-off" intermittency of the dynamo, as explored in detail by Alexakis & Ponty (2008) in the context of the ABC runs ABC1 and ABC2. These runs are notable for their short *off* phases, during which the magnetic field becomes weak enough to revert the system back to a hydrodynamic state. The dynamo comes back quickly, with a return to a MHD equilibrium (see Fig. 1 below). We thus finally have two different types of dynamo turbulence, with a large amount of fluctuations which are analyzed in the next section making use of their third and fourth-order normalized moment statistics using the full-space field data.

Run –	n_p	ν	R_V	R_λ	R_N	T_{max}	τ_{nl}	R_M	P_m	r
TG1 –	64	0.07	65.5	25.5	2.98	50×10^3	2.23	111	0.7	1.05
TG3 –	64	0.1	60.	24.3	3.35	130×10^3	1.86	430	3.3	5.26
ABC1 –	64	0.16	210.	45.8	2.4	60×10^3	1.14	32	1.45	1.18
ABC2 –	64	0.2	175.	41.	1.4	314.254×10^3	1.12	21	1.42	1.21

TABLE 1. Characteristics of the runs, with the linear resolution n_p of the cubic grid, ν the viscosity, the Reynolds number $R_V = LV_{rms}/\nu$, and Taylor Reynolds number $R_\lambda = \lambda V_{rms}/\nu$; $R_N = \eta_v n_p/3$ is the so-called Kaneda criterium based on the resolution in terms of the Kolmogorov dissipation length η_v. TG denotes Taylor-Green runs, and ABC denotes ABC runs (see text). T_{max} is the maximum time of the run, with the turn-over time τ_{nl} being of order 1 or 2 in terms of T_{max}. For the magnetic part, we give the magnetic Reynolds $R_M = LV_{rms}/\eta$, the magnetic Prandtl number $P_m = \nu/\eta$ and $r = R_M/R_M^C$ the ratio of the magnetic Reynolds number to the (approximate) critical value for the threshold of the dynamo. All these non-dimensional numbers need different definition of scales, like the integral scale $L = 2\pi \sum E(k)/k/\sum E(k)$ defined using the isotropic energy spectrum computed along the simulation at each wave number k, the Taylor scale $\lambda = \sqrt{10}\eta_v R_V^{1/4} = \sqrt{10} L_{int} R_V^{-1/2}$ in the inertial range, and the Kolmogorov scale $\eta_v = \left[\frac{\epsilon_v}{\nu^3}\right]^{-1/4} = L_{int} R_V^{-3/4}$ at the onset of the dissipation range. We need also one characteristic velocity which is usually taken as the root mean square of the kinetic energy $V_{rms} = \sqrt{2 \sum E(k)}$. The non-linear time is taken as $\tau_{nl} = L/V_{rms}$. All the scales and velocity are averaged in time as the simulations develop.

4. Analysis of the results

4.1. *Field gradient tensors, skewness and kurtosis*

Concerning the data points for measurements, which must be statistically independent, they are taken approximately every τ_{nl}; we recall that measurement errors go as $\sqrt{6/N_s}$ with N_s the number of independent data points (see *e.g.* Sura & Sardeshmukh (2008)). Large samples are needed also because a parabolic fit is quite sensitive to extreme values. Note that it is shown in Wan *et al.* (2010), in the context of two-dimensional (2D) MHD turbulence, that an estimate of the kurtosis at small scales requires, in the framework of the DNSs analyzed in that paper, that the (Kolmogorov) dissipation scale be at least twice as large as the cut-off $k_{max} = n_p/3$; this condition is well fulfilled by the runs of Table 3.1 (see parameter R_N).

We analyze the data using the point-wise rates of dissipation of the kinetic and magnetic energy given by $\epsilon_v(\mathbf{x}) = \mathbf{u} \cdot \partial_t \mathbf{u}$, $\epsilon_m(\mathbf{x}) = \mathbf{b} \cdot \partial_t \mathbf{b}$. They are expressed in terms of the symmetric part of the velocity gradient tensor, namely the strain tensor S_{ij}^v:

$$S_{ij}^v(\mathbf{x}) = \frac{\partial_j u_i(\mathbf{x}) + \partial_i u_j(\mathbf{x})}{2} \ , \ \epsilon_v(\mathbf{x}) = \Sigma_{ij} S_{ij}^v(\mathbf{x}) S_{ij}^v(\mathbf{x}) \ , \tag{4.1}$$

and of the magnetic current density, *viz.* $\epsilon_m(\mathbf{x}) = \mathbf{j}^2(\mathbf{x})$. For completion, we also define the symmetric part of the magnetic field gradient tensor, namely:

$$S_{ij}^m(\mathbf{x}) = \frac{\partial_j b_i(\mathbf{x}) + \partial_i b_j(\mathbf{x})}{2} \ , \ \sigma_m(\mathbf{x}) = \Sigma_{ij} S_{ij}^m(\mathbf{x}) S_{ij}^m(\mathbf{x}) \ . \tag{4.2}$$

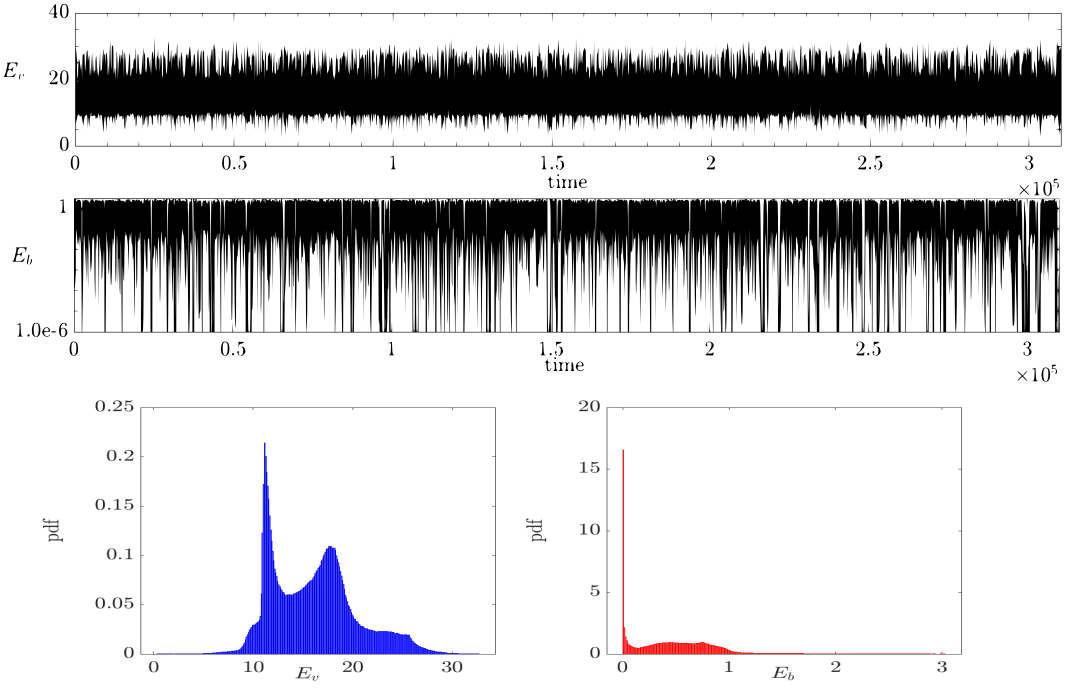

FIGURE 1. Run ABC2: temporal evolutions of the kinetic energy (blue, top) and magnetic energy (red, middle). Bottom: Probability density functions of the kinetic energy (left) and magnetic energy (right). Note the different units on the axes, and the lin-log scale for the magnetic energy.

Note that S_{ij}^m is a pseudo (axial) tensor. The integrated space-averaged, kinetic and magnetic energy dissipation rates and their sum can respectively be written as:

$$\epsilon_V = \nu \left\langle |\boldsymbol{\omega}|^2 \right\rangle \ , \ \epsilon_M = \ \eta \left\langle |\mathbf{j}^2| \right\rangle \ , \ \epsilon_T = \epsilon_V + \epsilon_M \ . \tag{4.3}$$

with $\boldsymbol{\omega} = \nabla \times \mathbf{u}$ the vorticity. Finally, the skewness and excess kurtosis are written below for a scalar field f, with $S_f = 0, K_f = 0$ for a Gaussian distribution, with the kurtosis (or flatness) being $F_f := K_f + 3$:

$$S_f = \left\langle f^3 \right\rangle / \left\langle f^2 \right\rangle^{3/2}, \ K_f = \left\langle f^4 \right\rangle / \left\langle f^2 \right\rangle^2 - 3 \ . \tag{4.4}$$

4.2. *Temporal and statistical data*

We give for the ABC2 flow (Figure 1) and for the TG3 case (Figure 2) the temporal evolution of the kinetic (top) and magnetic (middle) energy as a function of time; note that time is expressed in output counts, with a turn-over time being roughly twice that. At the bottom are given the energy PDFs for the velocity (left) and the magnetic field (right). In both cases, there are sustained fluctuations in the amplitude of the fields, and with in the case of the ABC run, lapses in both kinetic and magnetic energy corresponding to the on-off mechanism. This is directly related to the fact that the PDFs, in that case, have two relative maxima (with one peak close to zero for the magnetic field), whereas in the case of the TG forcing, the structure of the PDFs is simpler.

Fig. 3 gives $K(S)$ for various fields; at top, we display the $K(S)$ relationship for the z-component of the velocity, the square vorticity and the kinetic energy dissipation, namely $v_z(\mathbf{x}), \boldsymbol{\omega}^2(\mathbf{x})$ and $\epsilon_v(\mathbf{x})$; at bottom we plot the equivalent fields for the magnetic

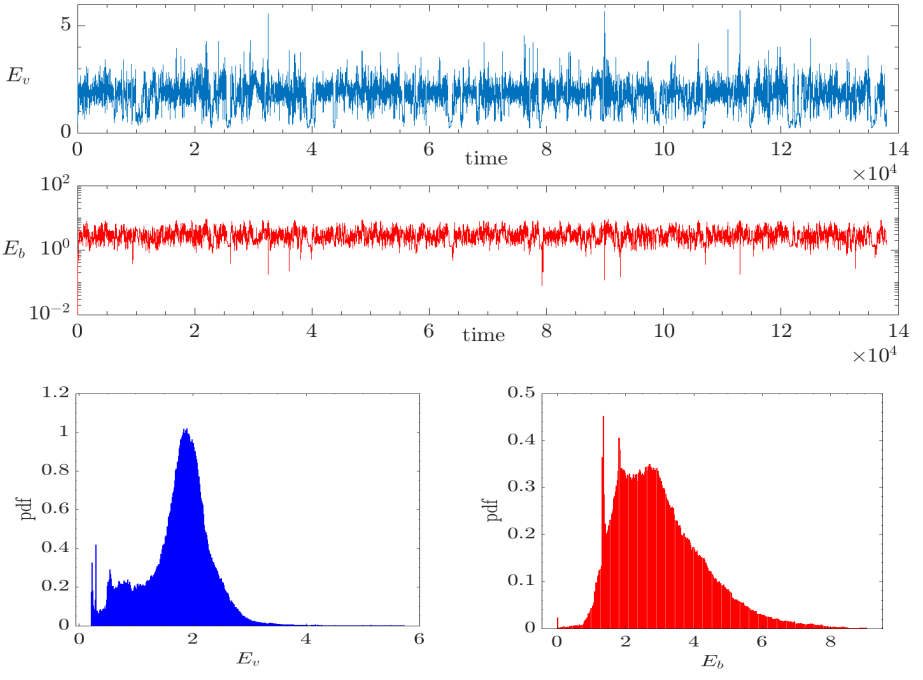

FIGURE 2. Run TG3: kinetic (top) and magnetic (middle) energy as a function of time. Bottom: Probability density function of the kinetic (left) and magnetic (right) energy.

induction, namely $b_z(\mathbf{x}), \sigma_m(\mathbf{x})$ and $j^2(\mathbf{x})$. The blue lines correspond to $K = [3/2][S^2 - 1]$ as mentioned before (see §2.1, and Sura & Sardeshmukh (2008)).

For each field variable, the data is collected roughly every turn-over time τ_{nl}, for in excess of 5×10^4 outputs, the time arrow of the data points being indicated by a rainbow color code as given by the color bar at left, with purple at early times and red at late times. For each temporal data point on these $K(S)$ plots, the space-dependent three-dimensional field we analyze is computed at each location in the n_p^3 data cube and its second, third and fourth moments are evaluated to construct skewness and kurtosis for that time index. Having in excess of 10^4 time stamps, the error on the skewness is less than 0.025, and twice that for the kurtosis.

We note the following: whereas for Navier-Stokes turbulence, the three components of the velocity field are Gaussian (Pouquet *et al.* (2023)), here the peak in values for K at $S \approx 0$ for v_z is up to $K \approx 6.5$, and rather narrowly centered around $S_{v_z} \approx 0$; high K values are also present for b_z. The hydrodynamic case analysed in Pouquet *et al.* (2023) is computed at comparable R_λ and n_p (but not T_M), and both S and K for the velocity are close to 0. On the other hand, for stratified flows with or without rotation, the vertical component of the velocity, v_z, can have high kurtosis and high values itself; this is associated with the intermittency of dissipation because of the variability of the system dominated by waves and all of a sudden developing small dissipative scales through shear-related instabilities. For this MHD run, the x and y components of the velocity behave approximately in the same way (not shown), with a skewness comparable to that of v_z but smaller K (with a maximum of ≈ 4 instead of 8), and similarly for b_x, b_y.

The symmetric and anti-symmetric parts of both the velocity and magnetic field gradient tensors have both high skewness and high kurtosis, and for them, a quasi-

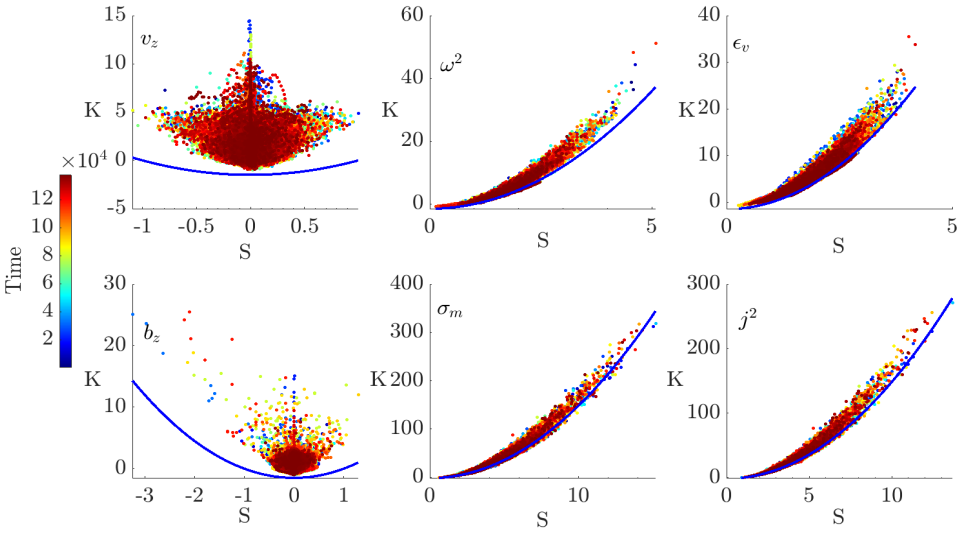

FIGURE 3. Top: For run TG3, $K(S)$ for the vertical velocity v_z (left), the square vorticity density $\boldsymbol{\omega}^2$ (middle), and the point-wise kinetic energy dissipation ϵ_v (right). Bottom: $K(S)$ for b_z (left), σ_m (middle), and j^2 (right). The color bar at left indicates the temporal clock in units of turn-over times, with early (late) times in blue (red). The blue lines follow $K(S) = 3/2[S^2 - 1]$.

parabolic fit is appropriate. The magnetic dissipation has higher kurtosis and thus is likely more intermittent than its kinetic counterpart, whereas vorticity dominates σ_m. On the other hand, both kinetic and magnetic dissipations have lower skewness and kurtosis than for the other part of their gradient tensors, although their statistics overall are similar. We recall that double exponential (Laplace), or Weibull distributions have small S of either sign and high kurtosis (Bertin & Clusel (2006); Biri *et al.* (2015); Aschwanden *et al.* (2016)). In that context, we note that it is shown in Sorriso-Valvo *et al.* (2018) that a proxy of energy transfer for the solar wind can be defined based on exact laws for MHD corresponding to the conservation of energy and cross-helicity $H_C = \langle \mathbf{v} \cdot \mathbf{b} \rangle$; these proxy fields display high intermittency in *Helios 2* (and Ulysses) data, with plausible stretched exponential fits. A final remark is that data points with $[K, S] \approx 0$ must be dominated by random noise at these times; they could correspond to relaxation intervals following sharp bursts in energy dissipation.

We now check whether this behavior is observed as well for another type of forcing. In Fig. 4 are plotted the $K(S)$ relationships at the top for v_z (left), $\boldsymbol{\omega}^2$ (middle) and ϵ_v (right) and (bottom), b_z (left), σ_m (middle) and j^2 (right), as in Fig. 3 but now for run ABC2 with a fully helical ABC forcing. Values for (S, K) for both runs are comparable except for the vertical component of the velocity due to its specific structure.

Finally, due to the strong symmetries of the initial conditions and forcing of the dynamos analyzed in this paper, one could wonder whether the addition of a small noise would change the results. On the other hand, in view of the length of the computations, well beyond what can be estimated for a reasonable Lyapounov time of separation of trajectories, it is unlikely that the overall results, and in particular the quasi-parabolic law for dissipation, would be altered. Indeed, one can find estimates of the first Lyapounov exponent λ_1, in the ABC dynamo for example, with $\lambda_1 \sim 0.073$ for a run with $R_V \approx$

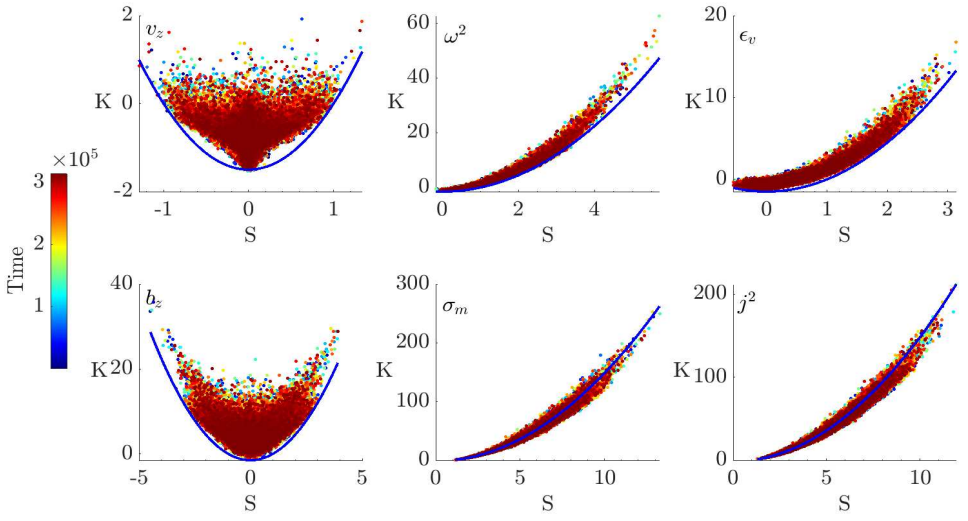

FIGURE 4. Same as Fig. 3 for run ABC2 with $R_V \approx 175$ and $T_{max} \approx 3.14 \times 10^5$.

60, $P_M = 4$, comparable to what we have here (Zienicke *et al.* (1998); Alexakis & Ponty (2008)), meaning that after roughly $14\tau_{nl}$, the initial conditions have been forgotten.

4.3. *Kurtosis-Skewness law as given by an intermittency model*

We can in fact compute the scaling exponent α_f in the relationship $K(S) \sim S^{\alpha_f}$, assuming the usual formulation for the structure functions of order p for a scalar field f, namely the field differences over a distance r, $\langle \delta f(r)^p \rangle \sim r^{\zeta_p}$; one obtains for α_f:

$$\alpha_f = \frac{\zeta_4 - 2\zeta_2}{\zeta_3 - \frac{3}{2}\zeta_2} \ . \tag{4.5}$$

Within the framework of the standard multi-fractal She & Lévêque (1994) (SL) model generalized for MHD in Grauer *et al.* (1994); Politano & Pouquet (1995), one has:

$$\zeta_p^{slf} = \frac{p}{9} + 2\left[1 - \left(\frac{2}{3}\right)^{p/3}\right] \ ; \ \alpha_{slf} = \frac{2[1 - 2(2/3)^{2/3} + (2/3)^{4/3}]}{7/3 - 3(2/3)^{2/3}} \approx 2.56 \ ; \tag{4.6}$$

$$\zeta_p^{slm} = \frac{p}{8} + 1 - \left(\frac{1}{2}\right)^{p/4} \ ; \ \alpha_{slm} = \frac{3 - 4(1/2)^{1/2}}{1 + 2(1/2)^{3/4} - 3(1/2)^{1/2}} \approx 2.53 \ . \tag{4.7}$$

In building these SL models for fluid turbulence (*slf*) and MHD (*slm*), an assumption is made that a hierarchy of flux structures exists compatible with a Kolmogorov transfer timescale and with vortex filaments (or in MHD, an isotropic Iroshnikov-Kraichnan wave-eddy interaction and current sheets). This leads to a specific non-linear relation in p for the ζ_ps. Note that a parabolic scaling, $\alpha = 2$, is obtained when considering the generalized versions of these log-Poisson models – derived in Politano & Pouquet (1995) both for fluids and for MHD – as the intermittency becomes maximal with extreme flux structures (see Pouquet *et al.* (2024)).

In this context, we compute power law fits, $|K| = \kappa |S|^\alpha$ (see Figs. 5 and 6) for the TG3 and ABC2 runs for the kinetic and magnetic dissipations, and for both full and

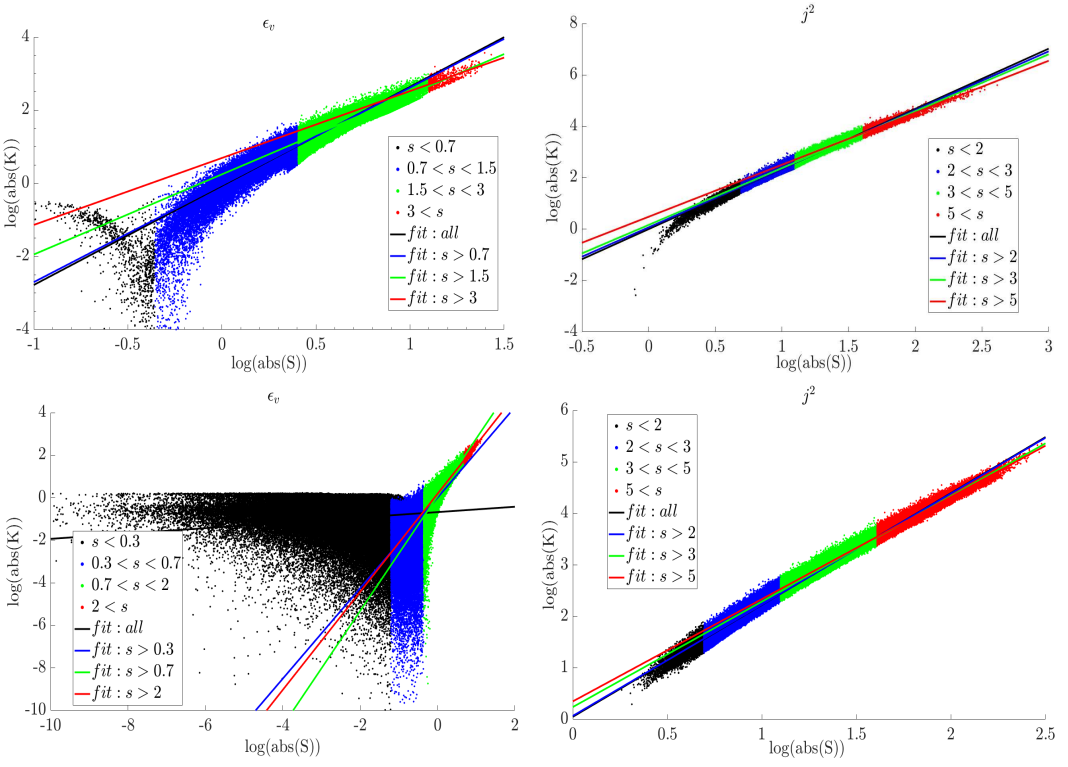

FIGURE 5. Log-log plot for $|K|(|S|) = \kappa|S|^\alpha$, runs TG3 (top) and ABC2 (bottom), for kinetic (left) and magnetic (right) dissipation. Thresholds in S are displayed in different colors.

thresholded data. There are clear variations of α with the strength of the intermittency as evaluated through the level of the skewness. Specifically, the chosen thresholds are $S < 2$ (black), $2 \leqslant S < 3$ (blue), $3 \leqslant S < 5$ (green) and $S \geqslant 5$ (red). Power-law fits in these intervals are given using the same colors. The high S, K values reached here are related to the very long integration times allowing for a thorough exploration of configuration space. We note that the velocity field has a broad range with non-intermittent values (black dots) in the sense that both S and K are quite low; it also undergoes a change of sign of the skewness at low values for TG3. We also observe that S and K can be substantially higher for j^2 than for the point-wise kinetic energy dissipation, and with less scatter for K at a given S. This difference might be related to the dynamo that controls the behavior of the magnetic field and its dissipation, whereas the velocity, at these resolutions, still feels the effect of the forcing, but the fit that includes these low-S points does not represent the behavior of the more intermittent data.

We give more quantitative information in Fig. 6, looking at variations with thresholds in skewness for the fit parameters of ϵ_V (first and third rows) and j^2 (second and fourth rows), for runs TG1 (solid blue lines) and TG3 (dashed red lines, first two rows), as well as for runs ABC1 (solid blue lines) and ABC2 (dashed red lines, last two rows). The α and κ coefficients are given in the first two columns, and the percentage of data points as a function of the threshold in skewness is in the third column; note that a 10% sample level still corresponds to 1.3×10^4 data points for TG3, and 3×10^4 points for ABC2.

We note first that the run TG3 has a higher R_M, and the two ABC runs have higher R_λ. The power-law index for ϵ_v has a substantially larger range of variation, with $0.2 \lesssim$

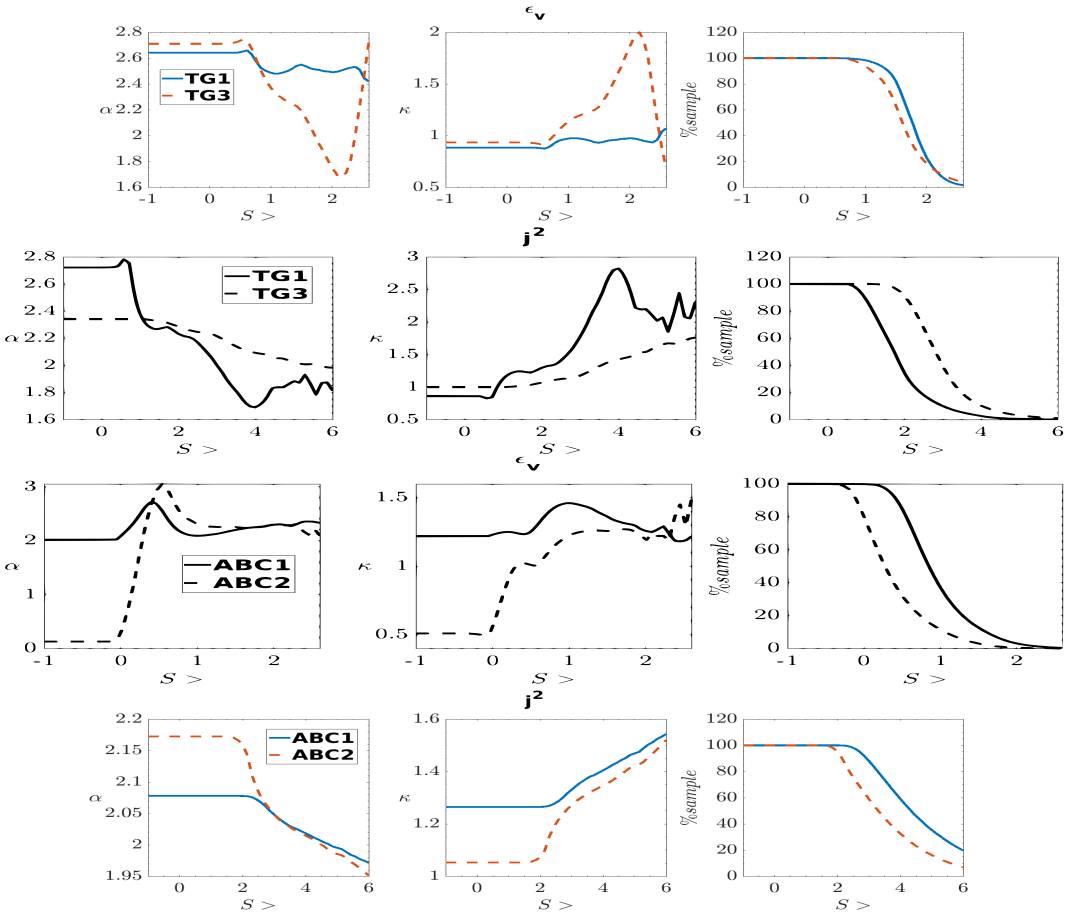

FIGURE 6. Given a fit $|K(S)| \sim \kappa |S|^\alpha$, variations with filter level in S of the parameters α (left), κ (middle) and the percentage of available data points per filter level in S (right), for ϵ_v (first and third rows) and j^2 (second and fourth rows), for the two TG runs (first two rows) and the two ABC runs (last two rows), with line and colors indicated in the inserts.

$\alpha_{\epsilon_v} \lesssim 3.0$ overall. For the current, α_{j^2} decreases systematically towards $\alpha_{j^2} \approx 2$ when the threshold in S is increased. If we exclude the points filtered with $S > 2$ for TG3 for which less than 10% of the data is relevant, we see a systematic decreasing trend in α towards a value of 2 or slightly lower, a value that can be recovered with the extension of the SL model to more varied dissipative structures (Pouquet *et al.* (2024)). The constant κ is of order unity in all cases, and increases with threshold as long as enough data is available. We also note its quasi-constancy at lower S values.

Indeed, a common feature of all these plots is that the variation with threshold in S starts abruptly at $1 \lesssim S$ for kinetic variables, and rather $2 \lesssim S$ for the magnetic ones for all the runs. This could indicate an effect on the velocity of the influence of the forcing at these moderate Reynolds numbers and that, at the modest Reynolds numbers achieved here, the velocity is not necessarily changed by the magnetic field which remains somewhat weak (see Figs. 1 and 2) and that for fluid turbulence, the skewness has a value of ≈ 0.5. Also, with the ratio $r < 5.3$ given in Table 3.1 indeed close to unity, we are still rather close to the threshold of the onset of the dynamo.

5. Discussion, conclusion and perspectives

We have found in this paper, for the fast dynamo regime, that a now classical quasi-parabolic behavior between kurtosis and skewness is present for kinetic and magnetic variables. The numerical data we analyzed represent but one aspect of the study of intermittency in the dynamo regime, and many questions remain. One issue concerns the effect a fully turbulent velocity will have on $K(S)$ scaling and the turbulence of the magnetic field itself. For example, using wavelets, Camporeale *et al.* (2018) could estimate in high-resolution 2D DNS of Hall-MHD that only 25% of the volume supports 50% of the energy transfer, giving thus a quantitative estimate of the intermittency of energy dissipation; we note that, for stratified fluids, this proportion can go as low as 11% of the kinetic energy dissipation for high kurtosis of the vertical velocity (Marino *et al.* (2022)). It will be of interest to examine as well these statistics in the case of fast dynamos at higher Reynolds numbers.

One might also want to study the role of cross-helicity H_C in the small scales, and in the nonlinear regime the role of magnetic helicity in the large scales, with $H_M = \langle \mathbf{A} \cdot \mathbf{b} \rangle$ and $\mathbf{b} = \nabla \times \mathbf{A}$. This requires sufficient scale separation in computations to be performed for long times, with forcing at an intermediate scale. Moreover, space plasmas are turbulent and, at small scale, magnetic reconnection plays an important role, although in the particular context of a $K(S)$ law, it is not known how reconnection would influence the specific scaling, nor how the introduction of small-scale kinetic effects would, but analysis of experiments in various plasma regimes do indicate the presence of such scaling laws.

Another issue is whether or not there is a dynamical consequence of $K(S)$ being close to its Cauchy-Schwarz limit. These inequalities linking K and S can be viewed as a limitation both on skewness (which has to be smaller than some value) and kurtosis, which cannot be too small. It shows that non-Gaussianity and intermittency are unavoidable (except for the trivial $(K = 0, S = 0)$ solution), but also that intermittency is limited in the sense that K and S are not independent, and at least for the NS case, the skewness is constrained by the exact law stemming from energy conservation (Kolmogorov (1941)), the laws in MHD involving cross-correlations (see for a recent review Marino & Sorriso-Valvo (2023)). Furthermore, as noted by several authors, $K(S)$ laws may put some limitation on the type of PDFs that a particular intermittent field follows. Similarly, some of these $K(S)$ relationships may contribute insight as to the relevance of Large Eddy Simulation (LES) parametrizations by providing constraints on the flow characteristics.

In view of a possible high Reynolds number universality of the $K_F(S_F)$ law for a variety of functionals F of the velocity and magnetic field, and within possible classes to be determined, as apply in particular to the dissipation, one can wonder whether a renormalization group (RNG) framework might be helpful. Such a theory has already been developed for fluid turbulence (Forster *et al.* (1976)), as well as for MHD, but it is not clear how one will approach the quest for the $K(S)$ relationship in that framework. One might further remark that the so-called model-A forcing $\sim k^2$ in the RNG corresponds to a Langevin model of the turbulence close to equilibrium in the case of a linearized version of the NS or MHD equations. It might well apply to the case of intermittency of the dissipative range (Kraichnan (1967)), but it is not clear how it would apply to the intermittency of the nonlinear inertial range.

The role of anisotropy in interpreting the dynamics of turbulent flows is complex, including at larger R_V such as that encountered in the atmosphere (Lovejoy *et al.* (2001)). For example, it is shown in Galtier (2023) that it affects in different ways the amplitude of the energy distribution and the spectral indices, so more work will

be needed in that direction as well; we already know that, for anisotropic fluid flows in the presence of stratification, the skewness and kurtosis of velocity components can be direction-dependent (Bos *et al.* (2007); see also Homann *et al.* (2014) for the fast dynamo), and that anisotropic scaling laws can be developed phenomenologically and found observationally (Nazarenko & Schekochihin (2011); Bian & Li (2024)).

When the velocity field is chaotic but not yet fully turbulent, and close to threshold for dynamo action, Sweet *et al.* (2001) identified a temporal bursty 'on-off" behavior of the dynamo-generated magnetic field which grows on average linearly with the control parameter, *i.e.* the distance in R_M from the threshold (see also Ponty *et al.* (2007); Alexakis & Ponty (2008), but these authors did not give indications on the behavior of the first few moments of the growing field). In Alexakis & Ponty (2008), the Lorentz force feed-back on the flow is studied in detail with DNS ran for up to $10^5\tau_{nl}$ and for various P_M; they find that the Lorentz force strongly modifies the temporal evolution of the growing field through a control of the noise. We already know that the noise can alter the coefficients in a parabolic relation (Theodorsen *et al.* (2017); Losada *et al.* (2023)), so we might be able to observe a change of scaling once we enter a turbulent saturation regime for the dynamo at higher Reynolds numbers, as we did for stratified flows (Pouquet *et al.* (2023)). This is left for future work.

Acknowledgements: Yannick Ponty thanks A. Miniussi for computing design assistance on the CUBBY code. The authors are grateful to the OPAL infrastructure from Université Côte d'Azur, the Université Côte d'Azur's Center for High-Performance Computing, and to the national French computer facilities (GENCI) for providing resources and support. Annick Pouquet is thankful to Bob Ergun for his encouragement.

REFERENCES

Adhikari, S., Shay, M. A., Parashar, T. N., Pyakurel, P. S., Matthaeus, W., Godzieba, D., Stawarz, J., Eastwood, J. P. & Dahlin, J. T. 2020 Reconnection from a turbulence perspective. *Phys. Plasmas* **27**, 042305.

Alexakis, A. & Ponty, Y. 2008 Effect of the Lorentz force on on-off dynamo intermittency. *Phys. Rev. E* **77**, 056308.

Aschwanden, M. J., Crosby, N. B., Dimitropoulou, M., Georgoulis, M. K., Hergarten, S., McAteer, J., Milovanov, A. V., Mineshige, S., Morales, L., Nishizuka, N., Pruessner, G., Sanchez, R., Sharma, A. S., Strugarek, A. & Uritsky, V. 2016 25 years of self-organized criticality: Solar and astrophysics. *Space Sci. Rev.* **198**, 47–166.

Balescu, R., Wang, H.-D. & Misguich, J. 1994 Langevin equation versus kinetic equation: Subdiffusive behavior of charged particles in a stochastic magnetic field. *Phys. Plasmas* **1**, 3826–3833.

Bandyopadhyay, R., Matthaeus, W. H. & Parashar, T. N. 2018 Single-mode nonlinear Langevin emulation of magnetohydrodynamic turbulence. *Phys. Rev. E* **97**, 053211.

Bertin, E. & Clusel, M. 2006 Generalized extreme value statistics and sum of correlated variables. *J. Phys. A* **39**, 7607–7619.

Bian, N. H. & Li, G. 2024 Lagrangian perspectives on the small-scale structure of Alfvénic turbulence and stochastic models for the dispersion of fluid particles and magnetic field lines in the solar wind. *APJ Supp.* **273**, 15.

Biri, S., Scharffenberg, M. G. & Stammer, D. 2015 A probabilistic description of the mesoscale eddy field in the ocean. *J. Geophys. Res.* **120**, 4778–4802.

Boldyrev, S. 2001 A solvable model for nonlinear mean field dynamo. *Astrophys. J.* **562**, 1081–1085.

Bos, W., Liechtenstein, L. & Schneider, K. 2007 Small-scale intermittency in anisotropic turbulence. *Phys. Rev.* **67**, 046310.

Bradshaw, Z., Farhat, A. & Grujic, Z. 2019 An algebraic reduction of the scaling gap in the navier-stokes regularity problem. *Arch. Rational Mech. Anal.* **231**, 1963–2005.

Brandenburg, A. & Subramanian, K. 2005 Astrophysical magnetic fields and nonlinear dynamo theory. *Phys. Rep.* **417** (1).

Buaria, D., Pumir, A. & Bodenschatz, E. 2022 Generation of intense dissipation in high reynolds number turbulence. *Phil. Trans. A* **380**, 20210088.

Camporeale, E., Sorriso-Valvo, L., Califano, F. & Retinó, A. 2018 Coherent structures and spectral energy transfer in turbulent plasma: A space-filter approach. *Phys. Rev. Lett.* **120** (125101).

Chen, C. 2016 Recent progress in astrophysical plasma turbulence from solar wind observations. *J. Plasma Phys.* **82**, 535820602.

Ergun, R. E., Ahmadi, N., Kromyda, L., Schwartz, S. J., Chasapis, A., Hoilijoki, S., Wilder, F. D., Stawarz, J. E., Goodrich, K. A., Turner, D. L., Cohen, I. J., Bingham, S. T., Holmes, J. C., Nakamura, R., Pucci, F., Torbert, R. B., Burch, J. L., Lindqvist, P.-A., Strangeway, R. J., Le Contel, O. & Giles, B. L. 2020 Observations of particle acceleration in magnetic reconnection–driven turbulence. *Astrophys. J.* **898**, 154.

Farago, J. 2002 Injected power fluctuations in Langevin equation. *J. Stat. Phys.* **107**, 781–803.

Farrell, B. & Ioannou, P. 2009 A theory of baroclinic turbulence. *J. Atmos. Sci.* **66**, 2444–2454.

Forster, D., Nelson, D. R. & Stephen, M. J. 1976 Long-time tails and the large-eddy behavior of a randomly stirred fluid. *Phys. Rev. Lett.* **36**, 867–870.

Furno, I., Avino, F., Bovet, A., Diallo, A., Fasoli, A., Gustafson, K., Iraji, D., Labit, B., Loizu, J., Müller, S. H., Plyushchev, G., Podesta, M., Poli, F. M., Ricci, P. & Theiler, C. 2015 Plasma turbulence, suprathermal ion dynamics and code validation on the basic plasma physics device torpex. *J. Plasma Phys.* **81**, 10.1017/S0022377815000161.

Galtier, S. 2023 Fast magneto-acoustic wave turbulence and the Iroshnikov-Kraichnan spectrum. *J. Plasma Phys.* **89**, 905890205.

Garcia, O. E. 2012 Stochastic modeling of intermittent scrape-off layer plasma fluctuations. *Phys. Rev. Lett.* **108**, 265001.

Grauer, R., Krug, J. & Mariani, C. 1994 Scaling of high-order structure functions in magnetohydrodynamic turbulence. *Phys. Lett. A* **195**, 335–338.

Guszejnov, D., Lazanyi, N., Bencze, A. & Zoletnik, S. 2013 On the effect of intermittency of turbulence on the parabolic relation between skewness and kurtosis in magnetized plasmas. *Phys. Plasmas* **20**, 112305.

Hasselmann, K. 1962 On the non-linear energy transfer in a gravity-wave spectrum. Part 1. General theory. *J. Fluid Mech.* **12**, 481–500.

Homann, H., Ponty, Y., Krstulovic, G. & Grauer, R. 2014 Structures and Lagrangian statistics of the Taylor-Green dynamo. *New J. Phys.* **16**, 075014.

Hughes, C. W., Thompson, A. F. & Wilson, C. 2010 Identification of jets and mixing barriers from sea level and vorticity measurements using simple statistics. *Ocean Mod.* **32**, 44–57.

Kolmogorov, A. N. 1941 Dissipation of energy in locally isotropic turbulence [English translation in Proc. Roy. Soc. London A 434 (1991) 15-17.]. *Dokl. Akad. Nauk SSSR* **32**, 19–21.

Kraichnan, R. H. 1967 Intermittency in the very small scales of turbulence. *Phys. Fluids* **10**, 2080–2082.

Kraichnan, R. H. & Nagarajan, S. 1967 Growth of turbulent magnetic fields. *Phys. Fluids* **10**, 859–870.

Krommes, J. A. 2008 The remarkable similarity between the scaling of kurtosis with squared skewness for TORPEX density fluctuations and sea-surface temperature fluctuations. *Phys. Plasmas* **15**, 030703.

Labit, B., Furno, I., Fasoli, A., Diallo, A., Müller, S., Plyushchev, G., Podestà, M. & Poli, F. 2007 Universal statistical properties of drift-interchange turbulence in TORPEX plasmas. *Phys. Rev. Lett.* **98**, 255002.

Lenschow, D., Mann, J. & Kristensen, L. 1994 How long is long enough when measuring fluxes and other turbulence statistics? *J. Atm. Oc. Tech.* **11**, 661–673.

Leprovost, N. & Dubrulle, B. 2005 The turbulent dynamo as an instability in a noisy medium. *Eur. Phys. J. B* **44**, 395–400.

Losada, J. M., Theodorsen, A. & Garcia, O. E. 2023 Stochastic modeling of blob-like plasma filaments in the scrape-off layer: Theoretical foundation. *Phys. Plasmas* **30**, 042518.

Lovejoy, S., Schertzer, D. & Stanway, J. D. 2001 Direct evidence of multifractal atmospheric cascades from planetary scales down to 1 km. *Phys. Rev. Lett.* **86**, 5200–5203.

Mallet, A., Schekochihin, A. A. & Chandran, B. D. 2017 Disruption of alfvénic turbulence by magnetic reconnection in a collisionless plasma. *JPP* **466**, 1–22.

Marino, R., Feraco, F., Primavera, L., Pumir, A., Pouquet, A. & Rosenberg, D. 2022 Turbulence generation by large-scale extreme drafts and the modulation of local energy dissipation in stably stratified geophysical flows. *Phys. Rev. F* **7**, 033801.

Marino, R. & Sorriso-Valvo, L. 2023 Scaling laws for the energy transfer in space plasma turbulence. *Physics Reports* **1006**, 1–144.

Matthaeus, W. H., Wan, M., Servidio, S., Greco, A., Osman, K. T., Oughton, S. & Dmitruk, P. 2015 Intermittency, nonlinear dynamics and dissipation in the solar wind and astrophysical plasmas. *Phil. Trans. R. Soc. A* **373**, 20140154.

Meneguzzi, M., Politano, H., Pouquet, A. & Zolver, M. 1996 A sparse-mode spectral method for the simulations of turbulent flows. *J. Comp. Phys.* **123**, 32–44.

Mezaoui, H., Hamza, A. & Jayachandran, P. 2014 Investigating high-latitude ionospheric turbulence using global positioning system data. *Geophys. Res. Lett.* **41**, 6570–6576.

Miranda, R. A., Schelin, A. B., Chian, A. C.-L. & Ferreira, J. L. 2018 Non-Gaussianity and cross-scale coupling in interplanetary magnetic field turbulence during a rope-rope magnetic reconnection event. *Ann. Geophys.* **36**, 497–507.

Nazarenko, S. & Schekochihin, S. 2011 Critical balance in magnetohydrodynamic, rotating and stratified turbulence: towards a universal scaling conjecture. *J. Fluid Mech.* **677**, 134–153.

Nazarenko, S. V., Falkovich, G. E. & Galtier, S. 2000 Feedback of a small-scale magnetic dynamo. *Phys. Rev. E* **63**, 016408.

Petoukhov, V., Eliseev, A., Klein, R. & Oesterle, H. 2008 On statistics of the free-troposphere synoptic component: an evaluation of skewnesses and mixed third-order moments contribution to the synoptic-scale dynamics and fluxes of heat and humidity. *Tellus* **60A**, 11–31.

Politano, H. & Pouquet, A. 1995 Model of intermittency in magnetohydrodynamic turbulence. *Phys. Rev. E* **52**, 636–641.

Politano, H., Pouquet, A. & Sulem, P. L. 1995 Current and vorticity dynamics in three–dimensional turbulence. *Phys. Plasmas* **2**, 2931–2939.

Ponty, Y., Laval, J., Dubrulle, B., Daviaud, F. & Pinton, J.-F. 2007 Subcritical dynamo bifurcation in the Taylor-Green flow. *Phys. Rev. Lett.* **99**, 224501.

Ponty, Y., Mininni, P. D., Montgomery, D., Pinton, J.-F., Politano, H. & Pouquet, A. 2005 Critical magnetic Reynolds number for dynamo action as a function of magnetic Prandtl number. *Phys. Rev. Lett.* **94**, 164502.

Pouquet, A., Marino, R., Politano, H., Ponty, Y. & Rosenberg, D. 2024 Intermittency in fluid and MHD turbulence analyzed through the prism of moment scaling predictions of multifractal models. *Nonlin. Proc. Geophys.* **In preparation**, xx.

Pouquet, A., Rosenberg, D., Marino, R. & Mininni, P. 2023 Intermittency scaling for mixing and dissipation in rotating stratified turbulence at the edge of instability. *Atmosphere* **14**, 01375.

Rafner, J., Grujic, Z., Bach, C., Bærentzen, J., Gervang, B., Jia, R.and Leinweber, S. & Misztal, M.and Sherson, J. 2021 Geometry of turbulent dissipation and the navier-stokes regularity problem. *Scientific Rep.* **11**, 8824.

Rincon, F. 2019 Dynamo theories. *J. Plasma Phys.* **85** (4).

Sattin, F., Agostini, M., Scarin, P., Vianello, N., Cavazzana, R., Marrelli, L., Serianni, G., Zweben, S. J., Maqueda, R., Yagi, Y., Sakakita, H., Koguchi, H., Kiyama, S., Hirano, Y. & Terry, J. 2009 On the statistics of edge fluctuations:

comparative study between various fusion devices. *Plasma Phys. Control. Fusion* **51**, 055013.

Schekochihin, A. A. 2022 MHD turbulence: A biased review. *J. Plasma Phys.* **88**, 155880501.

She, Z. & Lévêque, E. 1994 Universal scaling laws in fully developed turbulence. *Phys. Rev. Lett.* **72**, 336–339.

Sladkomedova, A., Cziegler, I., Field, A. R., Schekochihin, A. A. & Ivanov, P. G. 2023 Intermittency of density fluctuations and zonal-flow generation in MAST edge plasmas. *J. Plasma Phys.* **89**, 905890614 , 1–35.

Sorriso-Valvo, L., Carbone, F., Perri, S., Greco, A., Marino, R. & Bruno, R. 2018 On the statistical properties of turbulent energy transfer rate in the inner heliosphere. *Solar Phys.* **293**, 10.

Sura, P. & Sardeshmukh, P. D. 2008 A global view of non-gaussian SST variability. *J. Phys. Oceano.* **38**, 639–647.

Sweet, D., Ott, E., Antonsen, T. M., Lathrop, D. P. & Finn, J. M. 2001 Blowout bifurcations and the onset of magnetic dynamo action. *Phys. Plasmas* **8**, 1944–1952.

Theodorsen, A., Garcia, O. & Rypdal, M. 2017 Statistical properties of a filtered Poisson process with additive random noise: distributions, correlations and moment estimation. *Physica Scripta* **92**, 054002.

Wan, M., Oughton, S., Servidio, S. & Matthaeus, W. H. 2010 On the accuracy of simulations of turbulence. *Phys. Plasmas* **17**, 082308.

Watkins, N. W., Pruessner, G., Chapman, S. C., Crosby, N. B. & Jensen, H. J. 2016 Twenty-five years of Self-organized Criticality: Concepts and controversies. *Space Sci. Rev.* **198**, 3–44.

Wu, H., Huang, S., Wang, X., Yuan, Z., He, J. & Yang, L. 2023 Intermittency of magnetic discontinuities in the near-sun solar wind turbulence. *Astrophys. J. Lett.* **947**, L22.

Yeung, P. K., Zhai, X. M. & Sreenivasan, K. R. 2015 Extreme events in computational turbulence. *Proc. Nat. Acad. Sci.* **112**, 12633–12638.

Zhdankin, V., Boldyrev, S. & Mason, J. 2017 Influence of a large-scale field on energy dissipation in magnetohydrodynamic turbulence. *MNRAS* **468**, 4025–4029.

Zienicke, E., Politano, H. & Pouquet, A. 1998 Variable intensity of Lagrangian chaos in the nonlinear dynamo problem. *Phys. Rev. Lett.* **81**, 4640–4643.

Zwanzig, R. 1973 Nonlinear generalized Langevin equations. *J. Stat. Phys.* **9**, 215–220.